PERGAMON

International Journal of Solids and Structures 38 (2001) 1563–1583

INTERNATIONAL JOURNAL OF SOLIDS and STRUCTURES

www.elsevier.com/locate/ijsolstr

Comparison of wave propagation characteristics of the Cosserat continuum model and corresponding discrete lattice models

A.S.J. Suiker [a,*], A.V. Metrikine [b], R. de Borst [a]

[a] *Delft University of Technology, Koiter Institute Delft/Faculty of Aerospace Engineering, P.O. Box 5058, 2600 GB Delft, Netherlands*
[b] *Delft University of Technology, Faculty of Civil Engineering and Geosciences, P.O. Box 5048, 2600 GA Delft, Netherlands*

Received 17 September 1999; in revised form 13 March 2000

Abstract

A comparison is made between two-dimensional elastic discrete lattices and a corresponding Cosserat continuum. Firstly, it is demonstrated how the equations of motion of the Cosserat model can be retrieved from those of a lattice model. For this purpose, two lattice geometries are elaborated: a 7-cell hexagonal lattice and a 9-cell square lattice. For both lattices, the individual cells have two translational spring interactions and a rotational spring interaction with their neighbouring cells. Secondly, the dispersion relations for the lattice models and the Cosserat continuum model are examined in order to determine up to which wavelength of the deformation field the Cosserat model accurately represents the underlying discrete micro-structure. The effect of the lattice anisotropy and inhomogeneity on this accuracy is also discussed.

Keywords: Lattice models; Cosserat model; Wave propagation; Dispersion relations

1. Introduction

On the macroscopic level of observation, solid materials can be seen as a conglomerate of micro-structural elements that are adhesively interacting as a result of micro-structural forces. In correspondence with such a representation, the modelling of the mechanical behaviour of solid materials may be generally divided into two categories. Firstly, there are the discrete models, for which the equilibrium conditions, the kinematic conditions and the constitutive behaviour are formulated for each individual micro-structural element (=cell) with respect to its neighbouring micro-structural elements. Secondly, there are the continuum models, where the equilibrium conditions, the kinematic conditions and the constitutive behaviour are formulated for an assembly of micro-structural elements, using the continuum concepts of stress and strain.

* Corresponding author. Fax: +31-15-2611465.
E-mail address: a.suiker@lr.tudelft.nl (A.S.J. Suiker).

0020-7683/01/$ - see front matter
PII: S0020-7683(00)00104-9

A considerable advantage of discrete models in comparison to continuum models is that the *inhomogeneous effects* at the micro-level can be taken into account more accurately. However, the number of representative micro-structural elements in a macro-structural configuration is normally very large, which causes the number of equations that has to be solved for a discrete system to become large as well. For this reason, investigators have incorporated the inhomogeneous material behaviour in continuum formulations by *enhancing* the standard Boltzmann continuum with a 'characteristic material length'. This internal length scale is a macroscopic representation of the micro-structural parameters, such as the size of the micro-elements, the distribution of the micro-element contact forces and the geometry of the micro-structure.

A well-known enhanced continuum formulation is the *Cosserat continuum* (*or micro-polar continuum*), which is an augmentation of the standard Boltzmann continuum by three rotational degrees of freedom. The rotational degrees of freedom introduce a 'bending effect' in the constitutive formulations, and the characteristic length scale is therefore governed by the ratio between this additional bending stiffness and the normal stiffness. The development of the Cosserat continuum formulation started at the beginning of this century with the pioneering work of the Cosserats (Cosserat and Cosserat, 1909) in which the concept of the inclusion of rotational degrees of freedom was introduced for the first time. After a dormant period, this idea was picked up and further developed by a number of investigators (Günther, 1958; Schaefer, 1962; Mindlin, 1964; Toupin, 1964; Eringen, 1968). During the last decade, the Cosserat continuum model has been proven to be valuable in the analysis of localised failure problems (Mühlhaus and Vardoulakis, 1987; Mühlhaus, 1989; De Borst, 1991; De Borst and Sluys, 1992; Sluys, 1992; Groen, 1997), as well as in the analysis of wave propagation problems (Sluys, 1992; Erofeyev, 1992; Erofeyev and Potapov, 1993; Suiker et al., 1999a,b).

It is emphasised that the Cosserat model has been originally elaborated from the continuum concepts of stress and strain, and that it is not precisely clear up to which deformation level this continuum model accurately describes the underlying discrete micro-structure. Therefore, in this paper, two linear elastic discrete lattice models are compared with a corresponding Cosserat model. This is done via the analysis of the propagation characteristics of two-dimensional plane harmonic body waves. The discrete lattices that are considered are a 7-cell hexagonal lattice and a 9-cell square lattice, for which the individual cells are connected via translational springs in the longitudinal direction and in the shear direction, and a rotational spring. The inclusion of these three springs enables us to obtain the Cosserat model as a particular case of the lattice models. This would not be possible by considering lattices of only translational springs (Brillouin, 1946; Kosevich et al., 1996, Kosevich et al., 1998).

The Cosserat continuum model is derived from a long-wave approximation of the lattice models, which approach provides explicit relations between the macroscopic continuum parameters and the microscopic lattice parameters. The method of retrieving continuum models from lattice models has been discussed earlier by other investigators (Born and Huang, 1954; Maradudin et al., 1971). The work of Kunin (1983) also treats the relation between a discrete lattice and the Cosserat continuum. The cubic lattice that has been considered by him, consisting of masses that are connected by weightless rods, differs from those in the current paper. Additionally, Kunin's study focuses on the method of derivation, rather than on examining the quality of the results.

2. Governing equations for 7-cell hexagonal lattice

The two-dimensional discrete system that will be analysed first, is a so-called 7-cell hexagonal lattice, as depicted in Fig. 1. The inner cell (m,n) in this lattice is connected to six neighbouring cells at a distance d, via translational springs in the longitudinal direction K^n and in the shear direction K^s, and a rotational

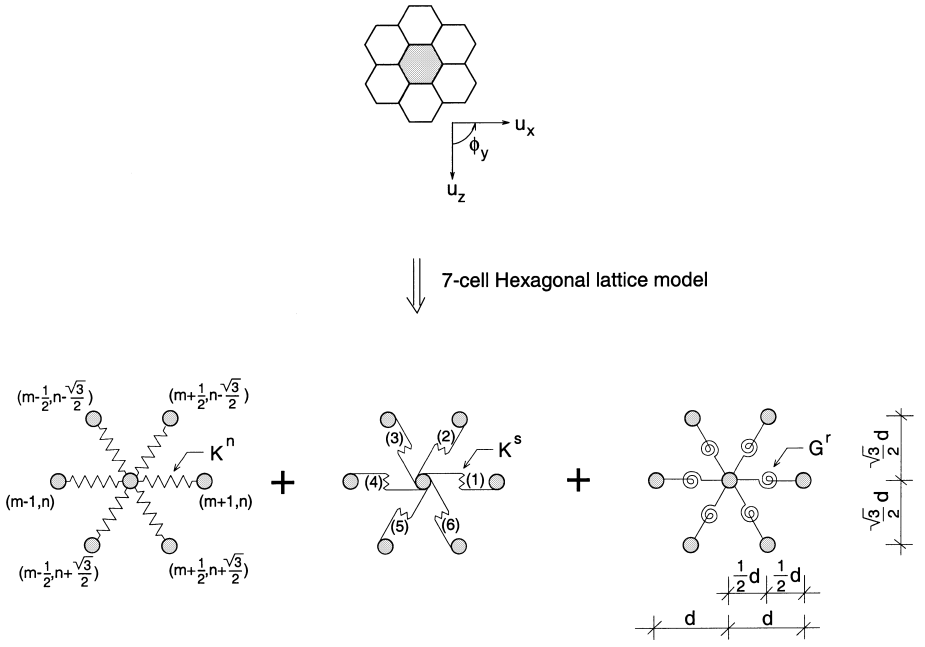

Fig. 1. Graphical representation of the 7-cell hexagonal lattice model.

spring G^{r}. In correspondence with the number of springs, each cell in this lattice has three degrees of freedom, namely a translation in the x direction and in the z direction, $\{u_x, u_z\}$, and a rotation in the y direction, ϕ_y.

The dynamic behaviour of the discrete lattice can be formulated via the Lagrangian L of the inner cell (m,n), which in a general form reads

$$L^{(m,n)} = E_{\mathrm{kin}}^{(m,n)} - E_{\mathrm{pot}}^{(m,n)} \tag{1}$$

with $E_{\mathrm{pot}}^{(m,n)}$ the potential energy and $E_{\mathrm{kin}}^{(m,n)}$ the kinetic energy. The potential energy of the inner cell may be written as

$$E_{\mathrm{pot}}^{(m,n)} = \frac{1}{2}\sum_{i=1}^{6}\left(\Delta l_{(i)}^2 K^n + \Delta s_{(i)}^2 K^{\mathrm{s}} + \Delta r_{(i)}^2 G^{\mathrm{r}}\right), \tag{2}$$

where $\Delta l_{(i)}$, $\Delta s_{(i)}$ and $\Delta r_{(i)}$ are the variations in length of the ith spring in the longitudinal direction, the shear direction and the rotational direction, respectively. For the hexagonal lattice, the linear form of these spring length variations has been presented in Appendix A. Additionally, the kinetic energy for the cell (m,n) is expressed as

$$E_{\mathrm{kin}}^{(m,n)} = \tfrac{1}{2}M\left(\dot{u}_x^{(m,n)}\right)^2 + \tfrac{1}{2}M\left(\dot{u}_z^{(m,n)}\right)^2 + \tfrac{1}{2}I\left(\dot{\phi}_y^{(m,n)}\right)^2 \tag{3}$$

with M the mass of the cell and I the moment of inertia. The dot on top of the degrees of freedom $\{u_x^{(m,n)}(t), u_z^{(m,n)}(t), \phi_y^{(m,n)}(t)\}$ denotes the full derivative with respect to time. When combining expressions

(1)–(3) with the spring length variations given in Appendix A, followed by applying the Lagrange equations (see for example, Landau and Lifshitz (1976))

$$\begin{aligned}
&\frac{\partial L^{(m,n)}}{\partial u_x^{(m,n)}} - \frac{\mathrm{d}}{\mathrm{d}t}\left(\frac{\partial L^{(m,n)}}{\partial \dot{u}_x^{(m,n)}}\right) = 0,\\
&\frac{\partial L^{(m,n)}}{\partial u_z^{(m,n)}} - \frac{\mathrm{d}}{\mathrm{d}t}\left(\frac{\partial L^{(m,n)}}{\partial \dot{u}_z^{(m,n)}}\right) = 0,\\
&\frac{\partial L^{(m,n)}}{\partial \phi_y^{(m,n)}} - \frac{\mathrm{d}}{\mathrm{d}t}\left(\frac{\partial L^{(m,n)}}{\partial \dot{\phi}_y^{(m,n)}}\right) = 0,
\end{aligned} \tag{4}$$

we obtain the equations of motion for the inner cell (m,n):

$$\begin{aligned}
M\ddot{u}_x^{(m,n)} = {} & \frac{1}{4}K^n\Big[-12u_x^{(m,n)} + 4u_x^{(m+1,n)} + 4u_x^{(m-1,n)} + u_x^{(m+1/2,n-\sqrt{3}/2)} + u_x^{(m-1/2,n-\sqrt{3}/2)}\\
& + u_x^{(m-1/2,n+\sqrt{3}/2)} + u_x^{(m+1/2,n+\sqrt{3}/2)} + \sqrt{3}u_z^{(m+1/2,n+\sqrt{3}/2)} + \sqrt{3}u_z^{(m-1/2,n-\sqrt{3}/2)}\\
& - \sqrt{3}u_z^{(m+1/2,n-\sqrt{3}/2)} - \sqrt{3}u_z^{(m-1/2,n+\sqrt{3}/2)}\Big]\\
& + \frac{\sqrt{3}}{4}K^{\mathrm{s}}\Big[-4\sqrt{3}u_x^{(m,n)} + \sqrt{3}u_x^{(m+1/2,n-\sqrt{3}/2)} + \sqrt{3}u_x^{(m-1/2,n-\sqrt{3}/2)} + \sqrt{3}u_x^{(m-1/2,n+\sqrt{3}/2)}\\
& + \sqrt{3}u_x^{(m+1/2,n+\sqrt{3}/2)} + u_z^{(m+1/2,n-\sqrt{3}/2)} - u_z^{(m-1/2,n-\sqrt{3}/2)} + u_z^{(m-1/2,n+\sqrt{3}/2)} - u_z^{(m+1/2,n+\sqrt{3}/2)}\\
& + d\Big(\phi_y^{(m+1/2,n-\sqrt{3}/2)} + \phi_y^{(m-1/2,n-\sqrt{3}/2)} - \phi_y^{(m-1/2,n+\sqrt{3}/2)} - \phi_y^{(m+1/2,n+\sqrt{3}/2)}\Big)\Big],
\end{aligned}$$

$$\begin{aligned}
M\ddot{u}_z^{(m,n)} = {} & \frac{\sqrt{3}}{4}K^n\Big[-4\sqrt{3}u_z^{(m,n)} + \sqrt{3}u_z^{(m+1/2,n-\sqrt{3}/2)} + \sqrt{3}u_z^{(m-1/2,n-\sqrt{3}/2)} + \sqrt{3}u_z^{(m-1/2,n+\sqrt{3}/2)}\\
& + \sqrt{3}u_z^{(m+1/2,n+\sqrt{3}/2)} - u_x^{(m+1/2,n-\sqrt{3}/2)} + u_x^{(m-1/2,n-\sqrt{3}/2)} - u_x^{(m-1/2,n+\sqrt{3}/2)} + u_x^{(m+1/2,n+\sqrt{3}/2)}\Big]\\
& + \frac{1}{4}K^{\mathrm{s}}\Big[-12u_z^{(m,n)} + 4u_z^{(m+1,n)} + 4u_z^{(m-1,n)} + u_z^{(m+1/2,n-\sqrt{3}/2)} + u_z^{(m-1/2,n-\sqrt{3}/2)}\\
& + u_z^{(m-1/2,n+\sqrt{3}/2)} + u_z^{(m+1/2,n+\sqrt{3}/2)} + \sqrt{3}u_x^{(m+1/2,n-\sqrt{3}/2)} - \sqrt{3}u_x^{(m-1/2,n-\sqrt{3}/2)}\\
& + \sqrt{3}u_x^{(m-1/2,n+\sqrt{3}/2)} - \sqrt{3}u_x^{(m+1/2,n+\sqrt{3}/2)} + d\Big(2\phi_y^{(m+1,n)} - 2\phi_y^{(m-1,n)} + \phi_y^{(m+1/2,n-\sqrt{3}/2)}\\
& - \phi_y^{(m-1/2,n-\sqrt{3}/2)} - \phi_y^{(m-1/2,n+\sqrt{3}/2)} + \phi_y^{(m+1/2,n+\sqrt{3}/2)}\Big)\Big],
\end{aligned} \tag{5}$$

$$\begin{aligned}
I\ddot{\phi}_y^{(m,n)} = {} & \frac{1}{4}K^{\mathrm{s}}\Big[d\Big(\sqrt{3}u_x^{(m-1/2,n+\sqrt{3}/2)} + \sqrt{3}u_x^{(m+1/2,n+\sqrt{3}/2)} - \sqrt{3}u_x^{(m-1/2,n-\sqrt{3}/2)}\\
& - \sqrt{3}u_x^{(m+1/2,n-\sqrt{3}/2)} + 2u_z^{(m-1,n)} + u_z^{(m-1/2,n-\sqrt{3}/2)} + u_z^{(m-1/2,n+\sqrt{3}/2)} - 2u_z^{(m+1,n)}\\
& - u_z^{(m+1/2,n-\sqrt{3}/2)} - u_z^{(m+1/2,n+\sqrt{3}/2)}\Big) - d^2\Big(6\phi_y^{(m,n)} + \phi_y^{(m+1,n)} + \phi_y^{(m+1/2,n-\sqrt{3}/2)}\\
& + \phi_y^{(m-1/2,n-\sqrt{3}/2)} + \phi_y^{(m-1,n)} + \phi_y^{(m-1/2,n+\sqrt{3}/2)} + \phi_y^{(m+1/2,n+\sqrt{3}/2)}\Big)\Big]\\
& + G^{\mathrm{r}}\Big[-6\phi_y^{(m,n)} + \phi_y^{(m+1,n)} + \phi_y^{(m+1/2,n-\sqrt{3}/2)} + \phi_y^{(m-1/2,n-\sqrt{3}/2)} + \phi_y^{(m-1,n)}\\
& + \phi_y^{(m-1/2,n+\sqrt{3}/2)} + \phi_y^{(m+1/2,n+\sqrt{3}/2)}\Big].
\end{aligned}$$

The *long-wave approximation* of the equations of motion (5) yields the equations of motion for the isotropic Cosserat continuum. The Cosserat continuum, as thoroughly discussed in the literature (see for example, Eringen (1968), Mühlhaus and Vardoulakis (1987), Mühlhaus (1989), De Borst (1991), De Borst and Sluys (1992), Sluys (1992), Suiker et al. (1999a), Suiker et al. (1999b)) is an augmentation of the standard Boltzmann continuum with three rotational degrees of freedom. The Cosserat continuum provides couple stresses that are energetically conjugated to the first-gradients of the rotation, which requires the introduction of additional constitutive coefficients. The equations of motion for a Cosserat continuum in the x–z coordinate system have the form (see for example Sluys (1992) and De Borst and Sluys (1992)):

$$\begin{aligned}
\rho\tilde{u}_{x,tt} &= (\lambda+2\mu)\tilde{u}_{x,xx} + \left(\lambda+\mu-\tfrac{1}{2}\kappa\right)\tilde{u}_{z,xz} + \left(\mu+\tfrac{1}{2}\kappa\right)\tilde{u}_{x,zz} - \kappa\tilde{\phi}_{y,z},\\
\rho\tilde{u}_{z,tt} &= (\lambda+2\mu)\tilde{u}_{z,zz} + \left(\lambda+\mu-\tfrac{1}{2}\kappa\right)\tilde{u}_{x,zx} + \left(\mu+\tfrac{1}{2}\kappa\right)\tilde{u}_{z,xx} + \kappa\tilde{\phi}_{y,x},\\
J\tilde{\phi}_{y,tt} &= 2\gamma\left(\tilde{\phi}_{y,xx}+\tilde{\phi}_{y,zz}\right) - 2\kappa\tilde{\phi}_{y} + \kappa\left(\tilde{u}_{x,z}-\tilde{u}_{z,x}\right)
\end{aligned} \tag{6}$$

with λ and μ the Lamé constants, κ and γ two additional constitutive coefficients that govern the 'bending effect', ρ the density and J the moment of inertia per unit volume. In Eq. (6), the tilde on top of the degrees of freedom designates that these degrees of freedom are continuous field variables. Subscripts x, z and t denote the partial derivatives with respect to the spatial coordinates x, z and time t. For deriving the equations of motion of the Cosserat model from that of the hexagonal lattice, the first step is to replace the discrete kinematic degrees of freedom by continuous field variables, i.e.

$$\{u_x^{(m,n)}, u_z^{(m,n)}, \phi_y^{(m,n)}\} \;\rightarrow\; \{\tilde{u}_x, \tilde{u}_z, \tilde{\phi}_y\}\Big|_{x=md,\, z=nd}. \tag{7}$$

The second step is to replace the degrees of freedom of the neighbouring cells, located at points $(x=(m+p)d,\ z=(n+q)d)$, by second-order Taylor approximations of the continuous field variables

$$\begin{aligned}
\{u_x^{(m+p,n+q)}, u_z^{(m+p,n+q)}, \phi_y^{(m+p,n+q)}\} \approx \Big\{ &\{\tilde{u}_x, \tilde{u}_z, \tilde{\phi}_y\} + pd\{\tilde{u}_{x,x}, \tilde{u}_{z,x}, \tilde{\phi}_{y,x}\} + qd\{\tilde{u}_{x,z}, \tilde{u}_{z,z}, \tilde{\phi}_{y,z}\}\\
&+ \tfrac{1}{2}\,p^2d^2\{\tilde{u}_{x,xx}, \tilde{u}_{z,xx}, \tilde{\phi}_{y,xx}\} + \tfrac{1}{2}\,q^2d^2\{\tilde{u}_{x,zz}, \tilde{u}_{z,zz}, \tilde{\phi}_{y,zz}\}\\
&+ pqd^2\{\tilde{u}_{x,xz}, \tilde{u}_{z,xz}, \tilde{\phi}_{y,xz}\}\Big\}\Big|_{x=md,\, z=nd}
\end{aligned} \tag{8}$$

in which p and q reflect the horizontal distance and vertical distance to neighbouring cells, respectively. When expressions (7) and (8) are substituted into the equations of motion (5), we obtain

$$M\tilde{u}_{x,tt} = \frac{9K^n+3K^s}{8}d^2\tilde{u}_{x,xx} + \frac{3(K^n-K^s)}{4}d^2\tilde{u}_{z,xz} + \frac{3K^n+9K^s}{8}d^2\tilde{u}_{x,zz} - \tfrac{3}{2}K^s d^2\tilde{\phi}_{y,z}, \tag{9a}$$

$$M\tilde{u}_{z,tt} = \frac{9K^n+3K^s}{8}d^2\tilde{u}_{z,zz} + \frac{3(K^n-K^s)}{4}d^2\tilde{u}_{x,zx} + \frac{3K^n+9K^s}{8}d^2\tilde{u}_{z,xx} + \tfrac{3}{2}K^s d^2\tilde{\phi}_{y,x}, \tag{9b}$$

$$I\tilde{\phi}_{y,tt} = \tfrac{3}{2}G^r d^2\left(\tilde{\phi}_{y,xx}+\tilde{\phi}_{y,zz}\right) - 3K^s d^2\tilde{\phi}_y + \tfrac{3}{2}K^s d^2\left(\tilde{u}_{x,z}-\tilde{u}_{z,x}\right), \tag{9c}$$

where in Eq. (9c) terms proportional to d^4 have been ignored. By comparing the equations of motion (9) with the equations of motion (6), it can be noticed that they are equal if, and only if, the following equalities hold:

$$M = \rho d^3, \tag{10a}$$

$$I = Jd^3, \tag{10b}$$

$$\frac{9K^n + 3K^s}{8d} = \lambda + 2\mu, \tag{10c}$$

$$\frac{3(K^n - K^s)}{4d} = \lambda + \mu - \tfrac{1}{2}\kappa, \tag{10d}$$

$$\frac{3K^n + 9K^s}{8d} = \mu + \tfrac{1}{2}\kappa, \tag{10e}$$

$$\frac{3K^s}{2d} = \kappa, \tag{10f}$$

$$\frac{3G^r}{2d} = 2\gamma. \tag{10g}$$

From the expressions (10), which relate the macroscopic continuum parameters to the microscopic lattice parameters, an expression for the shear modulus μ can be found by substituting Eq. (10f) into Eq. (10e). An expression for λ then follows from inserting the expression for μ either in Eq. (10c) or in Eq. (10d). This leads to

$$\begin{aligned} \lambda &= \frac{3(K^n - K^s)}{8d}, \\ \mu &= \frac{3(K^n + K^s)}{8d}. \end{aligned} \tag{11}$$

Hence, as long as the micro–macro relationships (10) are valid, the long-wave approximation of the equations of motion for the hexagonal lattice (9) equals the equations of motion of the Cosserat continuum (6). However, the question remains up to which level of deformation the equations of motion (5) and (9) describe the length and the frequency of a body wave in an equal manner. This issue will be discussed in Section 3.

3. Dispersion relations for body waves through hexagonal lattice and Cosserat continuum

To compare the dynamic behaviour of the hexagonal lattice and the Cosserat continuum, we will analyse the propagation of plane harmonic waves. For this wave type, the displacements $\{u_x^{(m,n)}, u_z^{(m,n)}\}$ and the rotation $\phi_y^{(m,n)}$ for the inner cell (m,n) of the hexagonal lattice have the form

$$\begin{aligned} u_x^{(m,n)} &= A \exp\left(i(\omega t - mk_x d - nk_z d)\right), \\ u_z^{(m,n)} &= B \exp\left(i(\omega t - mk_x d - nk_z d)\right), \\ \phi_y^{(m,n)} &= C \exp\left(i(\omega t - mk_x d - nk_z d)\right), \end{aligned} \tag{12}$$

where ω is the angular frequency of the wave, A, B and C are the wave amplitudes and k_x and k_z are the wave numbers in the x direction and z direction, respectively. The vector of wave numbers $\vec{k} = (k_x, k_z)$ is related to the vector of wavelengths $\vec{\Lambda} = (\Lambda_x, \Lambda_z)$ via the scalar product

$$\vec{k}\cdot\vec{\Lambda}=2\pi. \tag{13}$$

Also, the vector of wave numbers is related to the vector of phase velocities $\vec{c}=(c_x,c_z)$ via the scalar product

$$\vec{k}\cdot\vec{c}=\omega. \tag{14}$$

Substituting Eq. (12) into the equations of motion for the hexagonal lattice (5) yields a system of three algebraic equations:

$$\begin{aligned}
&A\Big[M\omega^2+K^n\Big(2\cos(k_xd)+\cos\big(\tfrac{1}{2}k_xd\big)\cos\Big(\tfrac{1}{2}\sqrt{3}k_zd\Big)-3\Big)+3K^s\Big(\cos\big(\tfrac{1}{2}k_xd\big)\cos\Big(\tfrac{1}{2}\sqrt{3}k_zd\Big)-1\Big)\Big]\\
&\quad+B\Big[-\sqrt{3}(K^n-K^s)\sin\big(\tfrac{1}{2}k_xd\big)\sin\Big(\tfrac{1}{2}\sqrt{3}k_zd\Big)\Big]+C\Big[\sqrt{3}K^sid\cos\big(\tfrac{1}{2}k_xd\big)\sin\Big(\tfrac{1}{2}\sqrt{3}k_zd\Big)\Big]=0,\\
&A\Big[-\sqrt{3}(K^n-K^s)\sin\big(\tfrac{1}{2}k_xd\big)\sin\Big(\tfrac{1}{2}\sqrt{3}k_zd\Big)\Big]+B\Big[M\omega^2+3K^n\Big(\cos\big(\tfrac{1}{2}k_xd\big)\cos\Big(\tfrac{1}{2}\sqrt{3}k_zd\Big)-1\Big)\\
&\qquad+K^s\Big(2\cos(k_xd)+\cos\big(\tfrac{1}{2}k_xd\big)\cos\Big(\tfrac{1}{2}\sqrt{3}k_zd\Big)-3\Big)\Big]\\
&\quad+C\Big[-K^sid\Big(\sin(k_xd)+\sin\big(\tfrac{1}{2}k_xd\big)\cos\Big(\tfrac{1}{2}\sqrt{3}k_zd\Big)\Big)\Big]=0,\\
&A\Big[-\sqrt{3}K^sid\cos\big(\tfrac{1}{2}k_xd\big)\sin\Big(\tfrac{1}{2}\sqrt{3}k_zd\Big)\Big]+B\Big[K^sid\Big(\sin(k_xd)+\sin\big(\tfrac{1}{2}k_xd\big)\cos\Big(\tfrac{1}{2}\sqrt{3}k_zd\Big)\Big)\Big]\\
&\quad+C\Big[I\omega^2-\tfrac{1}{2}K^sd^2\Big(\cos(k_xd)+2\cos\big(\tfrac{1}{2}k_xd\big)\cos\Big(\tfrac{1}{2}\sqrt{3}k_zd\Big)+3\Big)\\
&\qquad+2G^r\Big(\cos(k_xd)+2\cos\big(\tfrac{1}{2}k_xd\big)\cos\Big(\tfrac{1}{2}\sqrt{3}k_zd\Big)-3\Big)\Big]=0.
\end{aligned} \tag{15}$$

The system of equations (15) has a non-trivial solution if its determinant $\Delta(\omega,k_x,k_z)$ is equal to zero. By definition, the solutions of $\Delta(\omega,k_x,k_z)=0$ are called the dispersion relations of the (hexagonal lattice) system. For the Cosserat model, the equations that lead to the dispersion relations follow from substituting the harmonic solutions of the continuous form

$$\begin{aligned}
\tilde{u}_x&=A\exp\left(\mathrm{i}(\omega t-k_xx-k_zz)\right),\\
\tilde{u}_z&=B\exp\left(\mathrm{i}(\omega t-k_xx-k_zz)\right),\\
\tilde{\phi}_y&=C\exp\left(\mathrm{i}(\omega t-k_xx-k_zz)\right)
\end{aligned} \tag{16}$$

into the equations of motion (6), thereby using the micro–macro relationships (10). This yields

$$\begin{aligned}
&A\big[M\omega^2-(9K^n+3K^s)\tfrac{1}{8}k_x^2d^2-(3K^n+9K^s)\tfrac{1}{8}k_z^2d^2\big]+B\big[-(K^n-K^s)\tfrac{3}{4}k_xk_zd^2\big]+C\big[\tfrac{3}{2}K^sik_zd^2\big]=0,\\
&A\big[-(K^n-K^s)\tfrac{3}{4}k_xk_zd^2\big]+B\big[M\omega^2-(3K^n+9K^s)\tfrac{1}{8}k_x^2d^2-(9K^n+3K^s)\tfrac{1}{8}k_z^2d^2\big]+C\big[-\tfrac{3}{2}K^sik_xd^2\big]=0,\\
&A\big[-\tfrac{3}{2}K^sik_zd^2\big]+B\big[\tfrac{3}{2}K^sik_xd^2\big]+C\big[I\omega^2-3K^sd^2-\tfrac{3}{2}G^r\big(k_x^2+k_z^2\big)d^2\big]=0.
\end{aligned} \tag{17}$$

The dispersion relations of the hexagonal lattice and the Cosserat model, as obtained from numerically solving Eqs. (15) and (17), respectively, have been plotted in Fig. 2. Because the dispersion curves are symmetric with respect to $k=0$ and $\omega=0$, it is sufficient to plot only the parts that correspond to a positive wave number and a positive frequency. For the computation of the dispersion curves, the parameter set of Table 1 has been used, which constitutes a ballast material as used in ordinary railway tracks (Selig and Waters, 1994). Although the quality of the results will not depend on the characteristics of the material, the reason we have chosen for ballast is that the strong discrete nature of this material is an important influence factor in the high-frequency wave propagation in high-speed railway lines (Suiker et al., 1999b). The cell size d of the lattice has been set equal to the average particle diameter of the ballast. From the Lamé constants λ and μ and the average particle diameter d, the particle contact stiffness K^n and K^s have

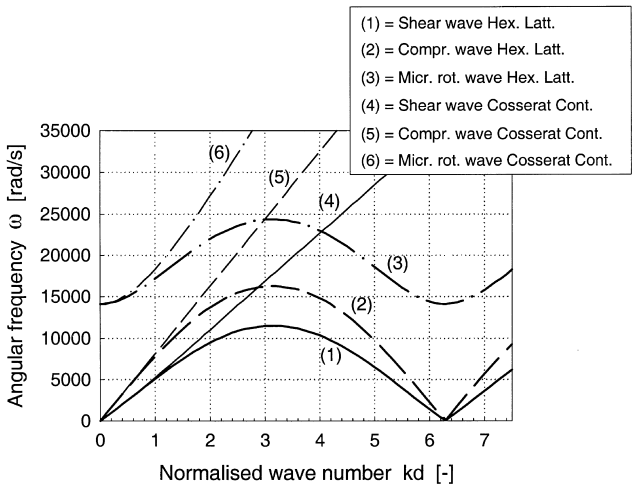

Fig. 2. The ω–kd dispersion curves for the 7-cell hexagonal lattice and the Cosserat continuum.

Table 1
Material parameters (ballast)

Lamé constants	
λ	55.5 MPa
μ	83.3 MPa
Density (ρ)	1800 kg/m^3
Particle diameter (d)	50 mm

been derived by inverting the relations (11). The rotational inertia has been calculated from the equation $I = 1/8Md^2$, assuming the particles to have a circular shape. As the literature does not provide values for the rotational stiffness of ballast particles, for simplicity reasons, we have chosen $G^{\mathrm{r}} = d^2K^{\mathrm{s}}$. It has to be mentioned, however, that this is an arbitrary choice, and that the rotational stiffness is strongly determined by the texture and shape of the ballast particles. Hence characteristics normally may differ for each individual particle.

For the dispersion curves in Fig. 2, the direction of propagation of the waves corresponds to $\{k_x, k_z\} = \{0, 2k/\sqrt{3}\}$, which for the hexagonal lattice results in a representation that reflects the so-called '*Brillouin zones*': $kd \in [-\pi, \pi] + [2\pi n, 2\pi(n+1)]$, with n an integer (for more details, see Brillouin (1946)). Fig. 2 illustrates that the hexagonal lattice as well as the Cosserat continuum transmits three types of waves: the compression wave, the shear wave, and the micro-rotational wave. In the long-wave limit $kd = 0$, for both models, the velocity of the shear wave and that of the compression wave are equal to those in a classic linear elastic solid:

$$\begin{aligned} &\text{Shear wave} \quad c_{\mathrm{sh},k=0} = \sqrt{\frac{(3K^n + 3K^{\mathrm{s}})d^2}{8M}} = \sqrt{\frac{\mu}{\rho}}, \\ &\text{Compression wave} \quad c_{\mathrm{compr},k=0} = \sqrt{\frac{(9K^n + 3K^{\mathrm{s}})d^2}{8M}} = \sqrt{\frac{\lambda + 2\mu}{\rho}}. \end{aligned} \tag{18}$$

Further, it can be noticed that up to a normalised wave number $kd \approx 1$, corresponding to a wavelength $\Lambda_z \approx 5.5d$, the overall agreement between the Cosserat continuum and the hexagonal lattice is good, in the

sense that the relative frequency difference between the continuum modes and the lattice modes is less than 5%. For smaller wave lengths, meaning higher normalised wave numbers, the dispersion curves of the Cosserat continuum model start to deviate from those of the hexagonal lattice model. This is mainly due to the increasing inhomogeneous effects that are caused by the cell distance. The description of inhomogeneous effects by a continuum formulation can nevertheless be further improved when increasing the order of the Taylor approximation (8) (Chang and Gao, 1995; Suiker et al., 2000a; Suiker et al., 2000b).

Another salient difference between the hexagonal lattice and the Cosserat continuum model is that for the lattice the anisotropy, as caused by the discrete nature of the micro-structure, becomes pronounced for short wavelengths. For the shear wave (Fig. 3), the compression wave (Fig. 4) and the micro-rotational

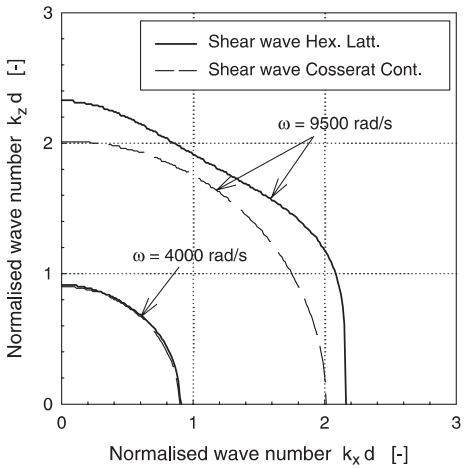

Fig. 3. Directional characteristics for the shear wave propagating through the hexagonal lattice and the Cosserat continuum; the normalised wave number $k_x d$ versus the normalised wave number $k_z d$ for two different frequencies ω.

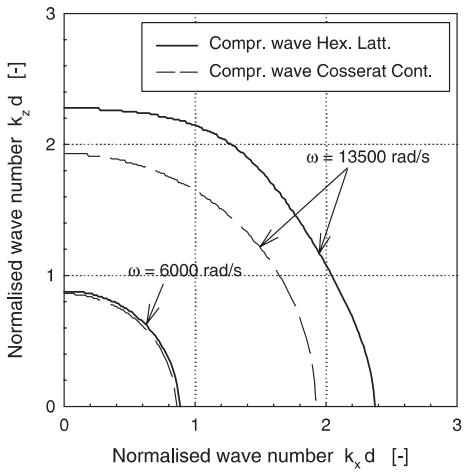

Fig. 4. Directional characteristics for the compression wave propagating through the hexagonal lattice and the Cosserat continuum; the normalised wave number $k_x d$ versus the normalised wave number $k_z d$ for two different frequencies ω.

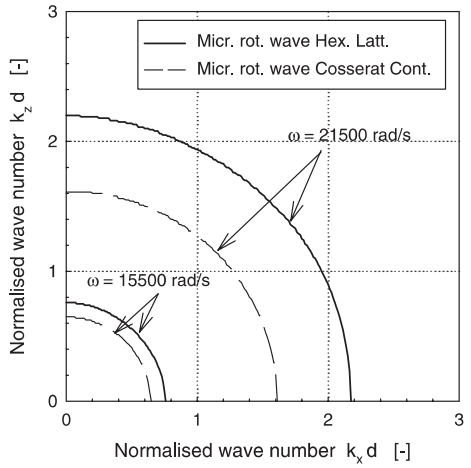

Fig. 5. Directional characteristics for the micro-rotational wave propagating through the hexagonal lattice and the Cosserat continuum; the normalised wave number $k_x d$ versus the normalised wave number $k_z d$ for two different frequencies ω.

wave (Fig. 5), this effect has been visualised by plotting the curves of constant frequency in the wave number plane $\{k_x, k_z\}$. These curves have been derived by determining the intersection points between the dispersion surface $\omega = \omega(k_x, k_z)$ and the specific plane $\omega =$ constant. The figures show that for the lower frequency, the hexagonal lattice behaves isotropically, leading to a circular shape of the k_x–k_z curves that also characterises the isotropic Cosserat continuum. For the higher frequency, the anisotropy causes the curves to lose circularity, although for the micro-rotational wave this effect appears to be minor. The overall difference between the curves for the Cosserat continuum and that for the hexagonal lattice in the high-frequency range is nevertheless not only the result of anisotropy aspects, but also of inhomogeneity aspects.

A characteristic that is not reflected by Figs. 3–5, but which is nevertheless due to the anisotropy, is that all wave types in the hexagonal lattice propagate in a coupled manner. This is different for the isotropic Cosserat continuum, where the compression wave propagates independently from the coupled propagation of the shear wave and the micro-rotational wave (Eringen, 1968; Sluys, 1992, Suiker et al., 2000b).

According to Fig. 2, for the Cosserat continuum the transmitted frequency of the three wave types may be infinite. On the contrary, the hexagonal lattice only transmits waves with a relatively low frequency, so that the lattice can be characterised as a 'granular filter'. The frequency maxima of the transmitted waves occur at a normalised wave number $kd = \pi$, which value bounds the first Brillouin zone (Brillouin, 1946). At this stage, the tangential slope of the lattice dispersion curves, which is a measure for the group velocity,

$$c_g = \frac{\partial \omega}{\partial k}, \tag{19}$$

turns from positive into negative. For unabsorbed travelling harmonic waves, the group velocity is equal to the energy velocity of the waves, where a positive value ($c_g > 0$) corresponds to a *positive dispersion*, and a negative value corresponds to a *negative dispersion*. At the transition between positive dispersion and negative dispersion, the group velocity is zero ($c_g = 0$), meaning that the wave energy does not propagate. Consequently, this wave may be called a *standing wave*. For all three wave types, a standing wave occurs at a wave number $kd = \pi$, corresponding to a wavelength $\Lambda = 2d$, see Fig. 2. As discussed in Brillouin (1946),

wavelengths smaller than two times the cell distance d should not be considered, since otherwise the relation between the wave number and the frequency is no longer unique. Also, the direction of wave propagation then becomes non-unique. Therefore, in this study only the ascending branch up to the point at which a standing wave occurs has been given a physical interpretation (first Brillouin zone).

4. Governing equations for 9-cell square lattice

In order to analyse the effect by the lattice geometry, apart from the 7-cell hexagonal lattice a second lattice will be considered, which is the 9-cell square lattice (Fig. 6). The inner cell (m,n) of this lattice is connected by axial springs to four neighbouring mid-side cells at a distance d, and by diagonal springs to four neighbouring edge cells at a distance $\sqrt{2}d$. The springs are of the longitudinal type $\{K^n_{\rm axi}, K^n_{\rm dia}\}$, of the shear type $\{K^{\rm s}_{\rm axi}, K^{\rm s}_{\rm dia}\}$ and of the rotational type $\{G^{\rm r}_{\rm axi}, G^{\rm r}_{\rm dia}\}$. As for the hexagonal lattice, each cell has three degrees of freedom: $\{u_x, u_z, \phi_y\}$.

Since the derivation procedure for the square lattice runs along the same lines as that for the hexagonal lattice, only the main expressions will be presented. The potential energy for the inner cell (m,n) can be derived as

$$E^{(m,n)}_{\rm pot} = \frac{1}{2}\sum_{i=1}^{4}\left(\Delta l^2_{(i)}K^n_{\rm axi} + \Delta s^2_{(i)}K^{\rm s}_{\rm axi} + \Delta r^2_{(i)}G^{\rm r}_{\rm axi}\right) + \frac{1}{2}\sum_{i=5}^{8}\left(\Delta l^2_{(i)}K^n_{\rm dia} + \Delta s^2_{(i)}K^{\rm s}_{\rm dia} + \Delta r^2_{(i)}G^{\rm r}_{\rm dia}\right), \tag{20}$$

where the variations of the spring length in the longitudinal direction, the shear direction and the rotational direction have been presented in Appendix B. The kinetic energy for the inner point (m,n) of the square lattice is equal to that of the hexagonal lattice, as given by expression (3). Combining the expressions (1), (3)

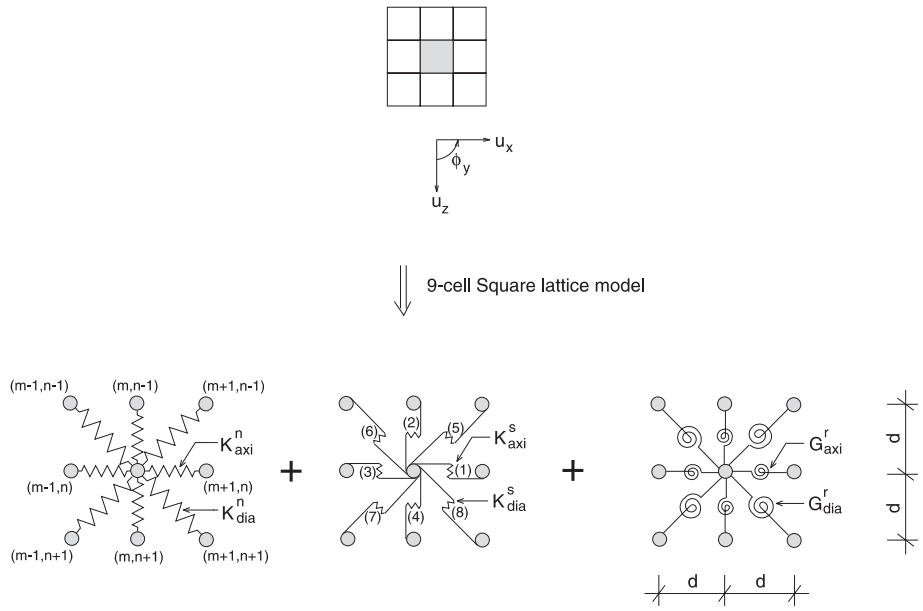

Fig. 6. Graphical representation of the 9-cell square lattice model.

and (20) with the spring length variations in Appendix B, followed by applying the Lagrange equations (4), yields

$$
\begin{aligned}
M\ddot{u}_x^{(m,n)} &= \frac{1}{2}K_{\mathrm{axi}}^{n}\big[-4u_x^{(m,n)}+2u_x^{(m+1,n)}+2u_x^{(m-1,n)}\big]\\
&\quad+\frac{1}{2}K_{\mathrm{dia}}^{n}\big[-4u_x^{(m,n)}+u_x^{(m+1,n+1)}+u_x^{(m+1,n-1)}+u_x^{(m-1,n+1)}+u_x^{(m-1,n-1)}\\
&\qquad+u_z^{(m+1,n+1)}+u_z^{(m-1,n-1)}-u_z^{(m+1,n-1)}-u_z^{(m-1,n+1)}\big]\\
&\quad+\frac{1}{2}K_{\mathrm{axi}}^{\mathrm{s}}\Big[-4u_x^{(m,n)}+2u_x^{(m,n+1)}+2u_x^{(m,n-1)}+d\Big(\phi_y^{(m,n-1)}-\phi_y^{(m,n+1)}\Big)\Big]\\
&\quad+\frac{1}{2}K_{\mathrm{dia}}^{\mathrm{s}}\big[-4u_x^{(m,n)}+u_x^{(m+1,n+1)}+u_x^{(m+1,n-1)}+u_x^{(m-1,n-1)}+u_x^{(m-1,n+1)}\\
&\qquad+u_z^{(m+1,n-1)}+u_z^{(m-1,n+1)}-u_z^{(m-1,n-1)}-u_z^{(m+1,n+1)}\\
&\qquad+d\Big(\phi_y^{(m+1,n-1)}+\phi_y^{(m-1,n-1)}-\phi_y^{(m+1,n+1)}-\phi_y^{(m-1,n+1)}\Big)\Big],\\
M\ddot{u}_z^{(m,n)} &= \frac{1}{2}K_{\mathrm{axi}}^{n}\big[-4u_z^{(m,n)}+2u_z^{(m,n+1)}+2u_z^{(m,n-1)}\big]\\
&\quad+\frac{1}{2}K_{\mathrm{dia}}^{n}\big[u_x^{(m+1,n+1)}+u_x^{(m-1,n-1)}-u_x^{(m+1,n-1)}-u_x^{(m-1,n+1)}\\
&\qquad-4u_z^{(m,n)}+u_z^{(m+1,n+1)}+u_z^{(m+1,n-1)}+u_z^{(m-1,n-1)}+u_z^{(m-1,n+1)}\big]\\
&\quad+\frac{1}{2}K_{\mathrm{axi}}^{\mathrm{s}}\Big[-4u_z^{(m,n)}+2u_z^{(m+1,n)}+2u_z^{(m-1,n)}+d\Big(\phi_y^{(m+1,n)}-\phi_y^{(m-1,n)}\Big)\Big]\\
&\quad+\frac{1}{2}K_{\mathrm{dia}}^{\mathrm{s}}\Big[u_x^{(m+1,n-1)}+u_x^{(m-1,n+1)}-u_x^{(m+1,n+1)}-u_x^{(m-1,n-1)}\\
&\qquad-4u_z^{(m,n)}+u_z^{(m+1,n+1)}+u_z^{(m+1,n-1)}+u_z^{(m-1,n+1)}+u_z^{(m-1,n-1)}\\
&\qquad+d\Big(\phi_y^{(m+1,n+1)}-\phi_y^{(m-1,n+1)}-\phi_y^{(m-1,n-1)}+\phi_y^{(m+1,n-1)}\Big)\Big],\\
I\ddot{\phi}_y^{(m,n)} &= \frac{1}{2}K_{\mathrm{axi}}^{\mathrm{s}}\Big[d\Big(u_x^{(m,n+1)}-u_x^{(m,n-1)}+u_z^{(m-1,n)}-u_z^{(m+1,n)}\Big)\\
&\qquad-\frac{1}{2}d^2\Big(4\phi_y^{(m,n)}+\phi_y^{(m+1,n)}+\phi_y^{(m-1,n)}+\phi_y^{(m,n+1)}+\phi_y^{(m,n-1)}\Big)\Big]\\
&\quad+\frac{1}{2}K_{\mathrm{dia}}^{\mathrm{s}}\Big[d\big(u_x^{(m+1,n+1)}+u_x^{(m-1,n+1)}-u_x^{(m-1,n-1)}-u_x^{(m+1,n-1)}\\
&\qquad+u_z^{(m-1,n+1)}+u_z^{(m-1,n-1)}-u_z^{(m+1,n+1)}-u_z^{(m+1,n-1)}\big)\\
&\qquad-d^2\Big(4\phi_y^{(m,n)}+\phi_y^{(m+1,n+1)}+\phi_y^{(m+1,n-1)}+\phi_y^{(m-1,n+1)}+\phi_y^{(m-1,n-1)}\Big)\Big]\\
&\quad+G_{\mathrm{axi}}^{\mathrm{r}}\Big[-4\phi_y^{(m,n)}+\phi_y^{(m+1,n)}+\phi_y^{(m-1,n)}+\phi_y^{(m,n-1)}+\phi_y^{(m,n+1)}\Big]\\
&\quad+G_{\mathrm{dia}}^{\mathrm{r}}\Big[-4\phi_y^{(m,n)}+\phi_y^{(m+1,n+1)}+\phi_y^{(m+1,n-1)}+\phi_y^{(m-1,n+1)}+\phi_y^{(m-1,n-1)}\Big].
\end{aligned}
\tag{21}
$$

Similar to the case of the 7-cell hexagonal lattice, expression (7) and the second-order Taylor approximation (8) are applied to the equations of motion (21) to give

$$M\tilde{u}_{x,tt} = \left(K^n_{\rm axi} + K^n_{\rm dia} + K^{\rm s}_{\rm dia}\right)d^2\tilde{u}_{x,xx} + 2\left(K^n_{\rm dia} + K^{\rm s}_{\rm dia}\right)d^2\tilde{u}_{z,xz} + \left(K^{\rm s}_{\rm axi} + K^n_{\rm dia} + K^{\rm s}_{\rm dia}\right)d^2\tilde{u}_{x,zz} - \left(K^{\rm s}_{\rm axi} + 2K^{\rm s}_{\rm dia}\right)d^2\tilde{\phi}_{y,z}, \tag{22a}$$

$$M\tilde{u}_{z,tt} = \left(K^n_{\rm axi} + K^n_{\rm dia} + K^{\rm s}_{\rm dia}\right)d^2\tilde{u}_{z,zz} + 2\left(K^n_{\rm dia} + K^{\rm s}_{\rm dia}\right)d^2\tilde{u}_{x,zx} + \left(K^{\rm s}_{\rm axi} + K^n_{\rm dia} + K^{\rm s}_{\rm dia}\right)d^2\tilde{u}_{z,xx} + \left(K^{\rm s}_{\rm axi} + 2K^{\rm s}_{\rm dia}\right)d^2\tilde{\phi}_{y,x}, \tag{22b}$$

$$I\tilde{\phi}_{y,tt} = \left(G^{\rm r}_{\rm axi} + 2G^{\rm r}_{\rm dia}\right)d^2\left(\tilde{\phi}_{y,xx} + \tilde{\phi}_{y,zz}\right) + 4G^{\rm r}_{\rm dia}d^2\tilde{\phi}_{y,xz} - 2\left(K^{\rm s}_{\rm axi} + 2K^{\rm s}_{\rm dia}\right)d^2\tilde{\phi}_y + \left(K^{\rm s}_{\rm axi} + 2K^{\rm s}_{\rm dia}\right)d^2\left(\tilde{u}_{x,z} - \tilde{u}_{z,x}\right), \tag{22c}$$

where the terms of the order d^4 have been omitted in Eq. (22c). Apparently, the long-wave approximation for the equations of motion of the square lattice model (22) equals the equations of motion of the Cosserat continuum model (6) under the following conditions:

$$M = \rho d^3, \tag{23a}$$

$$I = Jd^3, \tag{23b}$$

$$\frac{K^n_{\rm axi} + K^n_{\rm dia}}{d} = \lambda + 2\mu, \tag{23c}$$

$$\frac{2K^n_{\rm dia}}{d} = \lambda + \mu - \frac{1}{2}\kappa, \tag{23d}$$

$$\frac{K^n_{\rm dia} + K^{\rm s}_{\rm axi}}{d} = \mu + \frac{1}{2}\kappa, \tag{23e}$$

$$\frac{K^{\rm s}_{\rm axi}}{d} = \kappa, \tag{23f}$$

$$\frac{G^{\rm r}_{\rm axi}}{d} = 2\gamma, \tag{23g}$$

$$K^{\rm s}_{\rm dia} = 0, \tag{23h}$$

$$G^{\rm r}_{\rm dia} = 0. \tag{23i}$$

Obviously, the conditions (23h) and (23i) engender that for the shear and the rotational spring contributions only the axial part remains active, leading to the reduced square lattice model that has been depicted in Fig. 7. The expression for μ in terms of the discrete springs can now be found by substituting Eq. (23f) into Eq. (23e). Then, λ follows from combining Eqs. (23c) and (23e), as well as from combining Eq. (23d) with Eq. (23e):

$$\mu = \frac{2K^n_{\mathrm{dia}} + K^{\mathrm{s}}_{\mathrm{axi}}}{2d},$$
$$\lambda^{(1)} = \frac{K^n_{\mathrm{axi}} - K^n_{\mathrm{dia}} - K^{\mathrm{s}}_{\mathrm{axi}}}{d}, \tag{24}$$
$$\lambda^{(2)} = \frac{K^n_{\mathrm{dia}}}{d}.$$

The two different expressions for λ are the result of the anisotropic character of the square lattice, as caused by the different spring characteristics and the different cell distance in the axial and the diagonal direction. In order to return to an isotropic continuum in the long-wave approximation, it has to be required that the two expressions for λ in Eq. (24) are equal, which results in the constraint

$$2K^n_{\mathrm{dia}} = K^n_{\mathrm{axi}} - K^{\mathrm{s}}_{\mathrm{axi}}. \tag{25}$$

Combining Eqs. (25) and (24) then yields the Lamé constants

$$\lambda = \frac{K^n_{\mathrm{axi}} - K^{\mathrm{s}}_{\mathrm{axi}}}{2d},$$
$$\mu = \frac{K^n_{\mathrm{axi}}}{2d}. \tag{26}$$

Substituting the conditions (25), (23h) and (23i) into the equations of motion for the square lattice (21) gives

$$\begin{aligned}
M\ddot{u}_x^{(m,n)} &= K^n_{\mathrm{axi}}\Big[-3u_x^{(m,n)} + u_x^{(m+1,n)} + u_x^{(m-1,n)} \\
&\quad + \tfrac{1}{4}\big(u_x^{(m+1,n+1)} + u_x^{(m-1,n+1)} + u_x^{(m-1,n-1)} + u_x^{(m+1,n-1)}\big) \\
&\quad + \tfrac{1}{4}\big(u_z^{(m+1,n+1)} + u_z^{(m-1,n-1)} - u_z^{(m+1,n-1)} - u_z^{(m-1,n+1)}\big)\Big] \\
&\quad + K^{\mathrm{s}}_{\mathrm{axi}}\Big[-u_x^{(m,n)} + u_x^{(m,n+1)} + u_x^{(m,n-1)} \\
&\quad - \tfrac{1}{4}\big(u_x^{(m+1,n+1)} + u_x^{(m-1,n+1)} + u_x^{(m-1,n-1)} + u_x^{(m+1,n-1)}\big) \\
&\quad - \tfrac{1}{4}\big(u_z^{(m+1,n+1)} + u_z^{(m-1,n-1)} - u_z^{(m+1,n-1)} - u_z^{(m-1,n+1)}\big) \\
&\quad + \tfrac{1}{2}d\Big(\phi_y^{(m,n-1)} - \phi_y^{(m,n+1)}\Big)\Big], \\
M\ddot{u}_z^{(m,n)} &= K^n_{\mathrm{axi}}\Big[-3u_z^{(m,n)} + u_z^{(m,n+1)} + u_z^{(m,n-1)} + \tfrac{1}{4}\big(u_z^{(m+1,n+1)} + u_z^{(m+1,n-1)} \\
&\quad + u_z^{(m-1,n-1)} + u_z^{(m-1,n+1)}\big) + \tfrac{1}{4}\big(u_x^{(m+1,n+1)} + u_x^{(m-1,n-1)} \\
&\quad - u_x^{(m+1,n-1)} - u_x^{(m-1,n+1)}\big)\Big] + K^{\mathrm{s}}_{\mathrm{axi}}\Big[-u_z^{(m,n)} + u_z^{(m+1,n)} + u_z^{(m-1,n)} \\
&\quad - \tfrac{1}{4}\big(u_z^{(m+1,n+1)} + u_z^{(m+1,n-1)} + u_z^{(m-1,n-1)} + u_z^{(m-1,n+1)}\big) \\
&\quad - \tfrac{1}{4}\big(u_x^{(m+1,n+1)} + u_x^{(m-1,n-1)} - u_x^{(m+1,n-1)} - u_x^{(m-1,n+1)}\big) \\
&\quad + \tfrac{1}{2}d\Big(\phi_y^{(m+1,n)} - \phi_y^{(m-1,n)}\Big)\Big], \\
I\ddot{\phi}_y^{(m,n)} &= \tfrac{1}{2}K^{\mathrm{s}}_{\mathrm{axi}}\Big[d\big(u_x^{(m,n+1)} - u_x^{(m,n-1)} + u_z^{(m-1,n)} - u_z^{(m+1,n)}\big) \\
&\quad - \tfrac{1}{4}d^2\Big(4\phi_y^{(m,n)} + \phi_y^{(m+1,n)} + \phi_y^{(m-1,n)} + \phi_y^{(m,n+1)} + \phi_y^{(m,n-1)}\Big)\Big] \\
&\quad + G^{\mathrm{r}}_{\mathrm{axi}}\Big[-4\phi_y^{(m,n)} + \phi_y^{(m+1,n)} + \phi_y^{(m-1,n)} + \phi_y^{(m,n-1)} + \phi_y^{(m,n+1)}\Big].
\end{aligned} \tag{27}$$

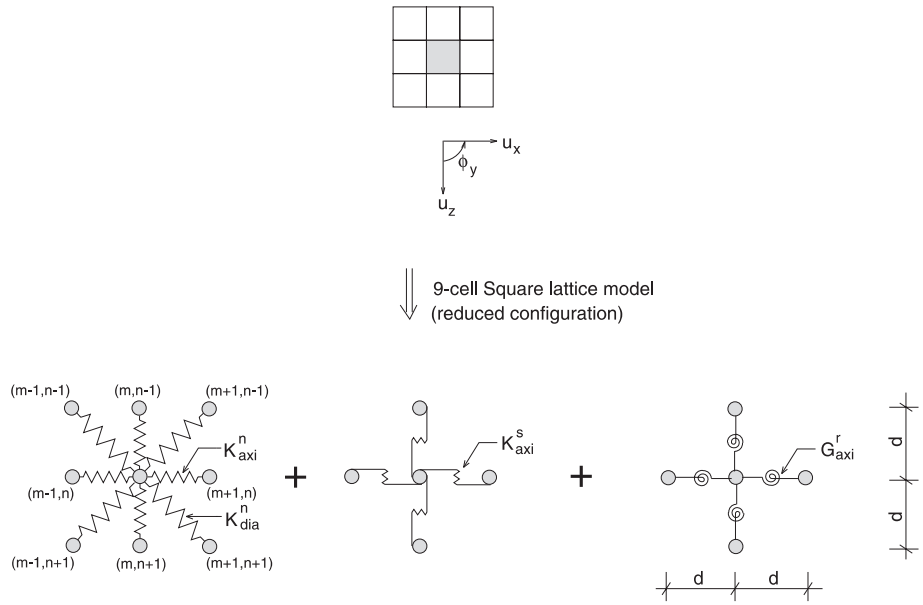

Fig. 7. Graphical representation of the 9-cell square lattice model: *the reduced configuration*.

5. Dispersion relations for body waves through square lattice and Cosserat continuum

For investigating the propagation of plane harmonic waves, we substitute the Eq. (12) into the equations of motion Eq. (27), which leads to

$$
\begin{aligned}
&A\big[M\omega^2 + K^n_{\mathrm{axi}}(2\cos(k_x d) + \cos(k_x d)\cos(k_z d) - 3) + K^{\mathrm{s}}_{\mathrm{axi}}(2\cos(k_z d)\\
&\quad - \cos(k_x d)\cos(k_z d) - 1)\big]\\
&\quad + B\big[(K^n_{\mathrm{axi}} - K^{\mathrm{s}}_{\mathrm{axi}})(-\sin(k_x d)(\sin(k_z d))\big]\\
&\quad + C\big[K^{\mathrm{s}}_{\mathrm{axi}} id\sin(k_z d)\big] = 0,\\
&A\big[(K^n_{\mathrm{axi}} - K^{\mathrm{s}}_{\mathrm{axi}})(-\sin(k_x d)\sin(k_z d))\big]\\
&\quad + B\big[M\omega^2 + K^n_{\mathrm{axi}}(2\cos(k_z d) + \cos(k_x d)\cos(k_z d) - 3) + K^{\mathrm{s}}_{\mathrm{axi}}(2\cos(k_x d)\\
&\quad - \cos(k_x d)\cos(k_z d) - 1)\big]\\
&\quad + C\big[-K^{\mathrm{s}}_{\mathrm{axi}} id\sin(k_x d)\big] = 0,\\
&A\big[-K^{\mathrm{s}}_{\mathrm{axi}} id\sin(k_z d)\big] + B\big[K^{\mathrm{s}}_{\mathrm{axi}} id\sin(k_x d)\big] + C\big[I\omega^2 + 2G^{\mathrm{r}}_{\mathrm{axi}}(\cos(k_x d) + \cos(k_z d) - 2)\\
&\quad - \tfrac{1}{2}K^{\mathrm{s}}_{\mathrm{axi}} d^2(\cos(k_x d) + \cos(k_z d) + 2)\big] = 0.
\end{aligned}
\tag{28}
$$

The dispersion relations for the square lattice can now be found by requiring the determinant of Eq. (28) to be equal to zero. Further, the set of equations that leads to the dispersion relations for the Cosserat model

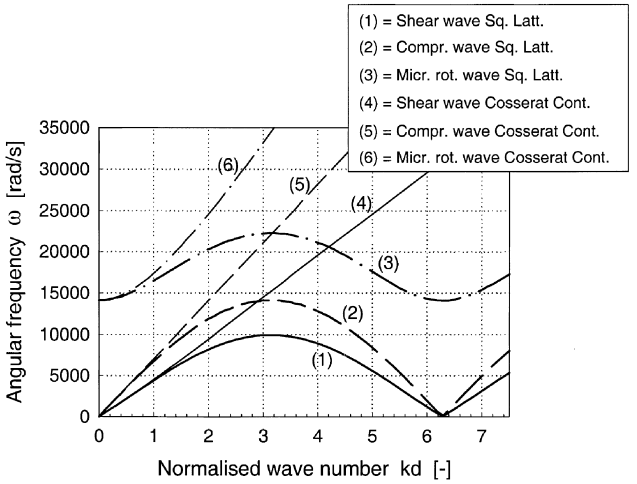

Fig. 8. The $\omega - kd$ dispersion curves for the 9-cell square lattice and the Cosserat continuum.

follows from substituting the harmonic forms (16) into the equations of motion (6), thereby using the micro–macro relationships (23) and the constraint (25):

$$\begin{aligned}
&A\left[M\omega^2 + \left(-3K^n_{\mathrm{axi}} + K^{\mathrm{s}}_{\mathrm{axi}}\right)\tfrac{1}{2}k_x^2 d^2 - \left(K^n_{\mathrm{axi}} + K^{\mathrm{s}}_{\mathrm{axi}}\right)\tfrac{1}{2}k_z^2 d^2\right] + B\left[-\left(K^n_{\mathrm{axi}} - K^{\mathrm{s}}_{\mathrm{axi}}\right)k_x k_z d^2\right] + C\left[K^{\mathrm{s}}_{\mathrm{axi}} i k_z d^2\right] = 0,\\
&A\left[-\left(K^n_{\mathrm{axi}} - K^{\mathrm{s}}_{\mathrm{axi}}\right)k_x k_z d^2\right] + B\left[M\omega^2 - \left(K^n_{\mathrm{axi}} + K^{\mathrm{s}}_{\mathrm{axi}}\right)\tfrac{1}{2}k_x^2 + \left(-3K^n_{\mathrm{axi}} + K^{\mathrm{s}}_{\mathrm{axi}}\right)\tfrac{1}{2}k_z^2 d^2\right] + C\left[-K^{\mathrm{s}}_{\mathrm{axi}} i k_x d^2\right] = 0,\\
&A\left[-K^{\mathrm{s}}_{\mathrm{axi}} i k_z d^2\right] + B\left[K^{\mathrm{s}}_{\mathrm{axi}} i k_x d^2\right] + C\left[I\omega^2 - 2K_s d^2 - G^{\mathrm{r}}_{\mathrm{axi}}\left(k_x^2 + k_z^2\right)d^2\right] = 0.
\end{aligned} \tag{29}$$

In Fig. 8, the dispersion relations for the square lattice and the Cosserat continuum are depicted, as calculated from the zero determinant of the sets of Eqs. (28) and (29), respectively. As for the hexagonal lattice, we have used the ballast material parameters in Table 1. The contact stiffness K_n^{axi} and K_s^{axi} have been derived from λ, μ and d by inverting the expressions (26). In order to retrieve the Brillouin zones, the direction of propagation of the body waves has been chosen in accordance with $(k_x, k_z) = (0, k)$. At the long-wave limit $kd = 0$, the shear wave velocity and the compression wave velocity are equal to the wave velocities in a classic elastic continuum:

$$\begin{aligned}
&\text{Shear wave} \quad c_{\mathrm{sh},k=0} = \sqrt{\frac{K^n_{\mathrm{axi}} d^2}{2M}} = \sqrt{\frac{\mu}{\rho}},\\
&\text{Compression wave } c_{\mathrm{compr},k=0} = \sqrt{\frac{\left(3K^n_{\mathrm{axi}} - K^{\mathrm{s}}_{\mathrm{axi}}\right)d^2}{2M}} = \sqrt{\frac{\lambda + 2\mu}{\rho}}.
\end{aligned} \tag{30}$$

These equations show that the wave velocities expressed in terms of micro-scale parameters differ from those of the hexagonal model (18), which comes from the different lattice geometry. Fig. 8 illustrates that the resemblance between the Cosserat model and the square lattice model is good up to a normalised wave

number $kd \approx 1$, corresponding to a wavelength $\Lambda_z \approx 6d$. This is approximately the same as for the hexagonal lattice ($\Lambda_z \approx 5.5d$).

Intuitively, the estimation of the minimum wavelength at which the Cosserat continuum model accurately describes the underlying micro-structure may be related to the direction in which the deformation takes place, as a result of the anisotropy of the lattice structure. However, by considering Figs. 3–5 for the hexagonal lattice together with Figs. 9–11 for the square lattice, it is obvious that the anisotropy only starts to play a role for wavelengths much shorter than $\Lambda_z \approx 6d$. Hence, it can be generally stated that elastic dynamic processes with spatial scales larger than six times the cell distance can be accurately described by

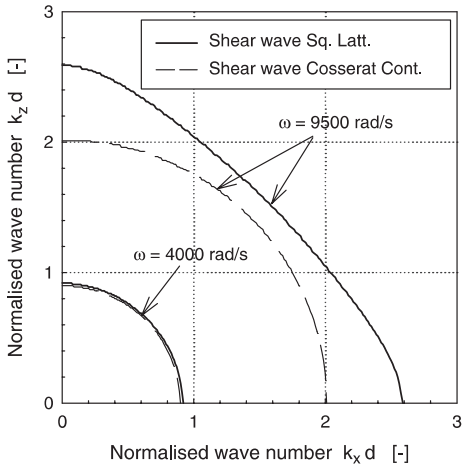

Fig. 9. Directional characteristics for the shear wave propagating through the square lattice and the Cosserat continuum; the normalised wave number $k_x d$ versus the normalised wave number $k_z d$ for two different frequencies ω.

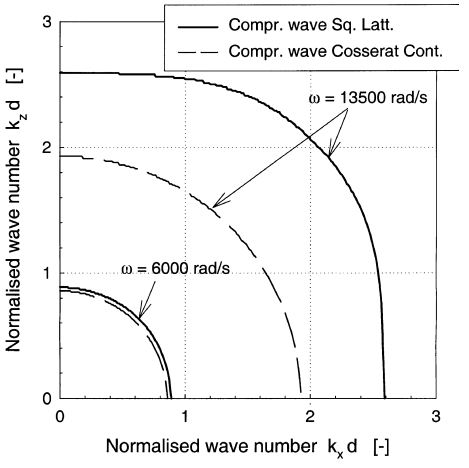

Fig. 10. Directional characteristics for the compression wave propagating through the square lattice and the Cosserat continuum; the normalised wave number $k_x d$ versus the normalised wave number $k_z d$ for two different frequencies ω.

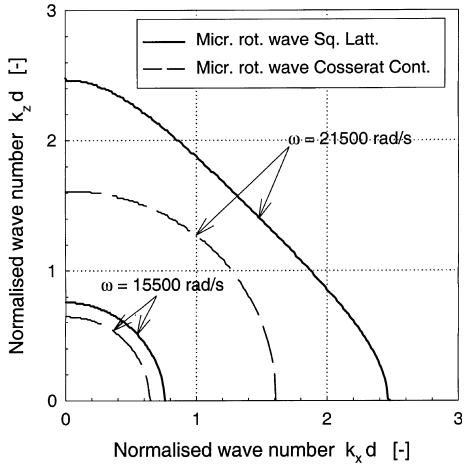

Fig. 11. Directional characteristics for the micro-rotational wave propagating through the square lattice and the Cosserat continuum; the normalised wave number $k_x d$ versus the normalised wave number $k_z d$ for two different frequencies ω.

an isotropic Cosserat continuum. For the analysis of shorter deformation patterns, a discrete lattice model should be used.

6. Conclusions

In this paper, the isotropic Cosserat continuum model has been compared with two different discrete models, which are the 7-cell hexagonal lattice and the 9-cell square lattice. The purpose of this comparison has been to examine up to which deformation level the Cosserat model accurately represents the specific underlying discrete micro-structure.

Via analysis of the dispersion curves, it has been demonstrated that the Cosserat model gives accurate results for deformation fields with a wavelength larger than approximately six times the micro-structural cell distance d. For shorter wavelengths, (strong) deviations occur as a result of the increasing inhomogeneity and anisotropy effects that are caused by the discrete nature of the micro-structure. Additionally, the filtering of the relatively high frequencies, which is a common feature of discrete lattice models, does not happen for the Cosserat model.

It has been further shown that the geometry of the discrete lattice structure strongly governs the format of the relationship between the micro-scale properties and the macro-scale properties, as well as the anisotropy and inhomogeneity characteristics in the short wavelength domain.

Although the Cosserat model gives unrealistic results in the domain of short wavelengths, the governing equations appear to be much less involved than those of a correspondent lattice model. Therefore, for boundary value problems in which wavelengths of a few times the particle size do not play a role, the Cosserat model may be a more appealing analysis tool than a lattice model.

Appendix A. Length variations of the springs in the hexagonal lattice

For the 7-cell hexagonal lattice in Fig. 1, the variations in length $\Delta l_{(i)}$, $\Delta s_{(i)}$ and $\Delta r_{(i)}$ in respectively the longitudinal direction, the shear direction and the rotational direction, are given by

$$\Delta l_{(1)} = u_x^{(m+1,n)} - u_x^{(m,n)},$$

$$\Delta l_{(2)} = \tfrac{1}{2}\Big(u_x^{(m+1/2,n-\sqrt{3}/2)} - u_x^{(m,n)} + \sqrt{3}\Big(u_z^{(m,n)} - u_z^{(m+1/2,n-\sqrt{3}/2)}\Big)\Big),$$

$$\Delta l_{(3)} = \tfrac{1}{2}\Big(u_x^{(m,n)} - u_x^{(m-1/2,n-\sqrt{3}/2)} + \sqrt{3}\Big(u_z^{(m,n)} - u_z^{(m-1/2,n-\sqrt{3}/2)}\Big)\Big),$$

$$\Delta l_{(4)} = u_x^{(m,n)} - u_x^{(m-1,n)},$$

$$\Delta l_{(5)} = \tfrac{1}{2}\Big(u_x^{(m,n)} - u_x^{(m-1/2,n+\sqrt{3}/2)} + \sqrt{3}\Big(u_z^{(m-1/2,n+\sqrt{3}/2)} - u_z^{(m,n)}\Big)\Big),$$

$$\Delta l_{(6)} = \tfrac{1}{2}\Big(u_x^{(m+1/2,n+\sqrt{3}/2)} - u_x^{(m,n)} + \sqrt{3}\Big(u_z^{(m+1/2,n+\sqrt{3}/2)} - u_z^{(m,n)}\Big)\Big),$$

$$\Delta s_{(1)} = \Big(u_z^{(m+1,n)} - u_z^{(m,n)} + \tfrac{1}{2}d\Big(\phi_y^{(m+1,n)} + \phi_y^{(m,n)}\Big)\Big),$$

$$\Delta s_{(2)} = \tfrac{1}{2}\Big(\sqrt{3}\Big(u_x^{(m+1/2,n-\sqrt{3}/2)} - u_x^{(m,n)}\Big) + u_z^{(m+1/2,n-\sqrt{3}/2)} - u_z^{(m,n)} + d\Big(\phi_y^{(m+1/2,n-\sqrt{3}/2)} + \omega_y^{(m,n)}\Big)\Big),$$

$$\Delta s_{(3)} = \tfrac{1}{2}\Big(\sqrt{3}\Big(u_x^{(m-1/2,n-\sqrt{3}/2)} - u_x^{(m,n)}\Big) + u_z^{(m,n)} - u_z^{(m-1/2,n-\sqrt{3}/2)} + d\Big(\phi_y^{(m-1/2,n-\sqrt{3}/2)} + \omega_y^{(m,n)}\Big)\Big),$$

$$\Delta s_{(4)} = \Big(u_z^{(m,n)} - u_z^{(m-1,n)} + \tfrac{1}{2}d\Big(\phi_y^{(m,n)} + \phi_y^{(m-1,n)}\Big)\Big),$$

$$\Delta s_{(5)} = \tfrac{1}{2}\Big(\sqrt{3}\Big(u_x^{(m,n)} - u_x^{(m-1/2,n+\sqrt{3}/2)}\Big) + u_z^{(m,n)} - u_z^{(m-1/2,n+\sqrt{3}/2)} + d\Big(\phi_y^{(m-1/2,n+\sqrt{3}/2)} + \phi_y^{(m,n)}\Big)\Big),$$

$$\Delta s_{(6)} = \tfrac{1}{2}\Big(\sqrt{3}\Big(u_x^{(m,n)} - u_x^{(m+1/2,n+\sqrt{3}/2)}\Big) + u_z^{(m+1/2,n+\sqrt{3}/2)} - u_z^{(m,n)} + d\Big(\phi_y^{(m+1/2,n+\sqrt{3}/2)} + \phi_y^{(m,n)}\Big)\Big),$$

$$\Delta r_{(1)} = \phi_y^{(m+1,n)} - \phi_y^{(m,n)},$$

$$\Delta r_{(2)} = \phi_y^{(m+1/2,n-\sqrt{3}/2)} - \phi_y^{(m,n)},$$

$$\Delta r_{(3)} = \phi_y^{(m-1/2,n-\sqrt{3}/2)} - \phi_y^{(m,n)},$$

$$\Delta r_{(4)} = \phi_y^{(m-1,n)} - \phi_y^{(m,n)},$$

$$\Delta r_{(5)} = \phi_y^{(m-1/2,n+\sqrt{3}/2)} - \phi_y^{(m,n)},$$

$$\Delta r_{(6)} = \phi_y^{(m+1/2,n+\sqrt{3}/2)} - \phi_y^{(m,n)}.$$

Appendix B. Length variations of the springs in the square lattice

For the 9-cell square lattice in Fig. 6, the variations in length $\Delta l_{(i)}$, $\Delta s_{(i)}$ and $\Delta r_{(i)}$ in respectively the longitudinal direction, the shear direction and the rotational direction are given by

$$
\begin{aligned}
\Delta l_{(1)} &= u_x^{(m+1,n)} - u_x^{(m,n)},\\
\Delta l_{(2)} &= u_z^{(m,n)} - u_z^{(m,n-1)},\\
\Delta l_{(3)} &= u_x^{(m,n)} - u_x^{(m-1,n)},\\
\Delta l_{(7)} &= u_z^{(m,n+1)} - u_z^{(m,n)},\\
\Delta l_{(5)} &= \tfrac{1}{2}\sqrt{2}\left(u_z^{(m,n)} - u_z^{(m+1,n-1)} - u_x^{(m,n)} + u_x^{(m+1,n-1)}\right),\\
\Delta l_{(6)} &= \tfrac{1}{2}\sqrt{2}\left(u_z^{(m,n)} - u_z^{(m-1,n-1)} - u_x^{(m-1,n-1)} + u_x^{(m,n)}\right),\\
\Delta l_{(7)} &= \tfrac{1}{2}\sqrt{2}\left(u_z^{(m-1,n+1)} - u_z^{(m,n)} - u_x^{(m-1,n+1)} + u_x^{(m,n)}\right),\\
\Delta l_{(8)} &= \tfrac{1}{2}\sqrt{2}\left(u_z^{(m+1,n+1)} - u_z^{(m,n)} - u_x^{(m,n)} + u_x^{(m+1,n+1)}\right),\\
\Delta s_{(1)} &= u_z^{(m+1,n)} - u_z^{(m,n)} + \tfrac{1}{2}d\left(\phi_y^{(m+1,n)} + \phi_y^{(m,n)}\right),\\
\Delta s_{(2)} &= u_x^{(m,n-1)} - u_x^{(m,n)} + \tfrac{1}{2}d\left(\phi_y^{(m,n)} + \phi_y^{(m,n-1)}\right),\\
\Delta s_{(3)} &= u_z^{(m,n)} - u_z^{(m-1,n)} + \tfrac{1}{2}d\left(\phi_y^{(m,n)} + \phi_y^{(m-1,n)}\right),\\
\Delta s_{(4)} &= u_x^{(m,n)} - u_x^{(m,n+1)} + \tfrac{1}{2}d\left(\phi_y^{(m,n+1)} + \phi_y^{(m,n)}\right),\\
\Delta s_{(5)} &= \tfrac{1}{2}\sqrt{2}\left(u_z^{(m+1,n-1)} - u_z^{(m,n)} - u_x^{(m,n)} + u_x^{(m+1,n-1)} + d\left(\phi_y^{(m+1,n-1)} + \phi_y^{(m,n)}\right)\right),\\
\Delta s_{(6)} &= \tfrac{1}{2}\sqrt{2}\left(u_z^{(m,n)} - u_z^{(m-1,n-1)} - u_x^{(m,n)} + u_x^{(m-1,n-1)} + d\left(\phi_y^{(m,n)} + \phi_y^{(m-1,n-1)}\right)\right),\\
\Delta s_{(7)} &= \tfrac{1}{2}\sqrt{2}\left(u_z^{(m,n)} - u_z^{(m-1,n+1)} - u_x^{(m-1,n+1)} + u_x^{(m,n)} + d\left(\phi_y^{(m,n)} + \phi_y^{(m-1,n+1)}\right)\right),\\
\Delta s_{(8)} &= \tfrac{1}{2}\sqrt{2}\left(u_z^{(m+1,n+1)} - u_z^{(m,n)} - u_x^{(m+1,n+1)} + u_x^{(m,n)} + d\left(\phi_y^{(m+1,n+1)} + \phi_y^{(m,n)}\right)\right),\\
\Delta r_{(1)} &= \phi_y^{(m+1,n)} - \phi_y^{(m,n)},\\
\Delta r_{(2)} &= \phi_y^{(m,n-1)} - \phi_y^{(m,n)},\\
\Delta r_{(3)} &= \phi_y^{(m-1,n)} - \phi_y^{(m,n)},\\
\Delta r_{(4)} &= \phi_y^{(m,n+1)} - \phi_y^{(m,n)},\\
\Delta r_{(5)} &= \phi_y^{(m+1,n-1)} - \phi_y^{(m,n)},\\
\Delta r_{(6)} &= \phi_y^{(m-1,n-1)} - \phi_y^{(m,n)},\\
\Delta r_{(7)} &= \phi_y^{(m-1,n+1)} - \phi_y^{(m,n)},\\
\Delta r_{(8)} &= \phi_y^{(m+1,n+1)} - \phi_y^{(m,n)}.
\end{aligned}
$$

References

Born, M., Huang, K., 1954. Dynamical Theory of Crystal Lattices. Clarendon Press, Oxford.

Brillouin, L., 1946. Wave Propagation in Periodic Structures. Dover, New York.

Chang, C.S., Gao, J., 1995. Second-gradient constitutive theory for granular material with random packing structure. Int. J. Solids Struct. 16, 2279–2293.

Cosserat, E., Cosserat, F., 1909. Théorie des Corps Deformables, Herman et fils, Paris.

Borst De, R., 1991. Simulation of strain localisation: A reappraisal of the Cosserat continuum. Engng. Comp. 8, 317–332.

Borst De, R., Sluys, L.J., 1992. Localisation in a Cosserat continuum under static and dynamic loading conditions. Comp. Meth. Appl. Mech. Engng. 90, 805–827.

Eringen, A.C., 1968. Theory of micro-polar elasticity. In: Liebowitz, H. (Ed.), Fracture – An Advanced Treatise, vol. II. Academic Press, New York, pp. 621–693.

Erofeyev, V.I., 1992. Resonance interactions of quasiharmonic waves in nonlinearly-elastic micropolar media. Accoust. Lett. 15, 131–135.

Erofeyev, V.I., Potapov, A.I., 1993. Longitudinal strain waves in nonlinearly-elastic media with couple stresses. Int. J. Non-lin. Mech. 28, 483–491.

Groen, A.E., 1997. Three-dimensional Elasto-plastic Analysis of Soils, Ph.D. Thesis. Delft University of Technology, The Netherlands.

Günther, W., 1958. Zur Statik und Kinematik des Cosseratschen Kontinuums. Abh. Braunschweig. Wiss. Ges. 10, 195–213.

Kosevich, A.M., Savotchenko, S.E., Matsokin, D.V., 1998. Surface and quasi-surface phonons and transformation waves in a hexagonal crystal. Low Temp. Phys. 24, 748–756.

Kosevich, A.M., Syrkin, E.S., Tutov, A.V., 1996. Acoustic shear waves localized near a planar defect in an fcc crystal. Low Temp. Phys. 22, 617–624.

Kunin, I.A., 1983. Elastic Media with Microstructure, vol. 2. Three-dimensional Models. Springer, Berlin.

Landau, L.D., Lifshitz, E.M., 1976. Mechanics. Pergamon, Oxford.

Maradudin, A.A., Montroll, E.M., Weiss, G.H., Ipatova, I.P., 1971. Theory of Lattice Dynamics in the Harmonic Approximation. Solid State Physics Suppl. 3. Academic Press, New York.

Mindlin, R.D., 1964. Micro-structure in linear elasticity. Arch. Ration. Mech. Anal. 16, 51–78.

Mühlhaus, H.-B., 1989. Application of Cosserat theory in numerical solutions of limit load problems. Ing.-Arch. 59, 124–137.

Mühlhaus, H.-B., Vardoulakis, I., 1987. The thickness of shear bands in granular materials. Géotechnique 37, 271–283.

Schaefer, H., 1962. Versuch einer Elastizitätstheorie des zweidimensionalen ebenen Cosserat-Kontinuums. In: Schäfer, M. (Ed.), Miszellaneen der Angewandten Mechanik. Akademie, Berlin, pp. 277–292.

Selig, E.T., Waters, J.M., 1994. Track Geotechnology and Substructure Management. Thomas Telford Services, London.

Sluys, L.J., 1992. Wave Propagation Localisation and Dispersion in Softening Solids, Ph.D. Thesis. Delft University of Technology, The Netherlands.

Suiker, A.S.J., Chang, C.S., De Borst, R., 2000a. Micro-mechanical modelling of granular material – Part 1 – Derivation of a second-gradient micro-polar constitutive theory. Acta Mech., in press.

Suiker, A.S.J., Chang, C.S., De Borst, R., 2000b. Micro-mechanical modelling of granular material – Part 2 – Plane wave propagation in infinite media. Acta Mech., in press.

Suiker, A.S.J., Chang, C.S., De Borst, R., Esveld, C., 1999a. Surface waves in a stratified half space with enhanced continuum properties – Part 1 – Formulation of the boundary value problem. Eur. J. Mech. A/Solids 18, 749–768.

Suiker, A.S.J., Chang, C.S., De Borst, R., Esveld, C., 1999b. Surface waves in a stratified half space with enhanced continuum properties – Part 2 – Analysis of the wave characteristics in regard to high-speed railway tracks. Eur. J. Mech. A/Solids 18, 769–784.

Toupin, R.A., 1964. Theory of elasticity with couple-stress. Arch. Ration. Mech. Anal. 17, 85–112.